Optimizing Silicon-Plasmonic Waveguides for $\chi^{(3)}$ Nonlinear Applications

Alexandros Pitilakis, Odysseas Tsilipakos and Emmanouil E. Kriezis

Department of Electrical and Computer Engineering,
Aristotle University of Thessaloniki, Thessaloniki, Greece
*corresponding author, E-mail: alexpiti@auth.gr

Abstract

Hybrid silicon-plasmonic waveguides constitute an appealing platform for integrated photonic circuitry. They merge the technical maturity and prevalence of the SOI platform with the subwavelength confinement of plasmonic waveguides, essential for accessing enhanced nonlinear response at micron length-scales. Employing full-wave numerical simulations complemented with Schrödinger equation techniques, we propose nonlinear waveguide designs for Kerr-effect applications exhibiting minimized impairments due to free-carrier effects, thus raising the power-ceiling imposed on standard silicon waveguides.

1. Introduction

Nonlinear phenomena emanating from the third order susceptibility $\chi^{(3)}$ hold the key to efficient all-optical signal processing in integrated photonics. Circuitry based on standard silicon-on-insulator (SOI) waveguides [1] presents limited potential for micron-length-scale Kerr-type nonlinear applications due to the large interaction length-scales required: typically longer than 1 mm [2, 3]. Furthermore, silicon exhibits two-photon absorption (TPA) in the telecom band, which in turn, apart from introducing additional losses, gives rise to free-carrier effects (FCEs), namely dispersion (FCD) and, more importantly, absorption (FCA). The magnitude of FCEs increases quadratically with the optical power. Thus, FCA limits the maximum on-chip average power to a few tens of milliwatts; above this threshold, it drastically quenches the optical power. On the other hand, purely plasmonic waveguides [4] can allow for subwavelength confinement significantly boosting the nonlinear response and thus reducing the required interaction length. However, they suffer from substantial Ohmic losses, a fundamental barrier for any nonlinear application .

Hybrid silicon-plasmonic (HSP) waveguides [5] present a fair compromise between silicon and plasmonic traits, with respect to the potential for Kerr-type nonlinear applications [6]. Fusing index-contrast and plasmonic guiding mechanisms, they confine the optical field in a nanosized low-index dielectric gap, formed between a metal and a high-index silicon area. If the dielectric additionally possesses a high nonlinear index n_2, then the nonlinear parameter γ quantifying the Kerr-effect strength acquires orders-of-magnitude larger values than those typical of SOI waveguides ($\gamma \approx 100\ \mathrm{m^{-1}W^{-1}}$). More importantly, HSP waveguides offer a two-fold advantage over SOI ones with respect to FCE impairments. Specifically, as the optical field is confined primarily inside the dielectric gap, not only is the relative TPA magnitude (r_{TPA}) decreased, but, in addition, TPA-generated free-carriers (residing only inside the silicon area) do not significantly overlap with the optical field. These two aspects mean that the overall FCE perturbation is considerably decreased, even further than nonlinear-slot waveguides [3]. In view of these attributes, HSP waveguides offer increased potential for Kerr-related nonlinear applications in compact integrated photonic components at length scales in the order of tens of microns, while also allowing for higher on-chip powers, if that is necessary.

2. Nonlinear Figure-of-Merit

In order to establish a common ground for the comparison of nonlinear waveguides, we define a figure-of-merit (FoM) that provides a qualitative measure of the impact of all discussed nonlinear phenomena, namely, the Kerr effect, TPA and FCEs. We start off with a basic FoM for TPA-free waveguides defined as

$$\mathcal{F} = \gamma \times L_{\mathrm{prop}} = \gamma/\alpha \tag{1}$$

and measured in $\mathrm{W^{-1}}$. In this equation, $L_{\mathrm{prop}} = 1/\alpha$ is the propagation length, i.e., the e-folding distance of the optical power, due to linear propagation losses (α). The nonlinear parameter (γ) is the real-part of its complex-valued counterpart

$$\gamma_c = \frac{3\omega\varepsilon_0}{4\mathcal{N}^2} \sum_{\mu,\alpha,\beta,\gamma}^{x,y,z} \iint_{\infty} \chi^{(3)}_{\mu\alpha\beta\gamma} e^*_\mu e_\alpha e^*_\beta e_\gamma \, dxdy, \tag{2}$$

that is rigorously extracted [2] from the electric-field distribution ($\mathbf{e}$) and the cross-sectional profile of the $\chi^{(3)}$-tensor. The latter has a real and an imaginary part, associated with the Kerr-index (n_2) and the TPA-coefficient (β_{TPA}), respectively [1]. Finally, $\mathcal{N}$ is a normalization-integral quantifying the axial power-flow $\mathcal{N} = \mathrm{Re}\{\iint (\mathbf{e} \times \mathbf{h}^*) \cdot \hat{\mathbf{z}}\, dxdy\}$.

It can be shown that the input-power (P_{in}) required for a particular Kerr-type nonlinear application is proportional to $1/\mathcal{F}$. For instance, when the waveguide length is fixed at $L = L_{\mathrm{prop}}$, then spectral FWHM-doubling of

a guassian pulse requires $P_{\text{in}} \approx 4/\mathcal{F}$, nonlinear switching (due to desynchronization) of a directional coupler occurs at $P_{\text{in}} \approx 9/\mathcal{F}$, and a given degenerate four-wave-mixing (FWM) efficiency η requires a CW pump power of $P_{\text{in}} \approx 3\eta^{0.5}/\mathcal{F}$ [3].

Subsequently, in order to evaluate the influence of TPA and FCEs, a power-dependent FoM can be derived according to $\mathcal{F}' = \gamma' \times L'_{\text{prop}}$. For this purpose, the effective quantities γ' and L'_{prop} are introduced by applying correction terms to the nonlinear parameter and propagation length, respectively. These correction terms scale with the input-power and are derived from a nonlinear Schrödinger equation (NLSE) formulation [2] and, more specifically, from the phase and amplitude of the complex-envelope of a signal propagating along a nonlinear waveguide. Both primed quantities are smaller than the respective non-primed ones; FCD counteracts the self-focusing Kerr-effect leading to a reduced effective nonlinear parameter ($\gamma' < \gamma$), while both TPA and FCA are responsible for additional losses that lower the effective propagation length ($L'_{\text{prop}} < L_{\text{prop}}$). The defined $\mathcal{F}'$ is useful when studying how the Kerr-performance of a particular waveguide deteriorates under the effect of TPA and FCE as the power level increases. However, when optimizing or comparing different waveguides it is useful to quantify the relative importance of FCEs; it can be shown that the latter increases with the dimensionless FCE scaling factor

$$f_{\text{fc}} = r_{\text{TPA}} \times \Pi_{\text{Si}} \tag{3}$$

where r_{TPA} is the tangent of the complex-valued nonlinear parameter of Eq. (2), i.e., $r_{\text{TPA}} = \text{Im}\{\gamma_c\}/\text{Re}\{\gamma_c\}$, and Π_{Si} is the fraction of the optical-intensity residing inside silicon-areas of the cross-section

$$\Pi_{\text{Si}} = \frac{\iint_{\text{Si}} |\mathbf{e}|^2 \, dxdy}{\iint_{\infty} |\mathbf{e}|^2 \, dxdy} \leq 1. \tag{4}$$

For typical SOI-waveguides, where the light is guided mostly inside the Si-core, $r_{\text{TPA}} \approx 0.25$ and $\Pi_{\text{Si}} > 0.5$ [2] leading to $f_{\text{fc}} > 0.1$. On the contrary, HSP waveguides are expected to have considerably smaller values of f_{fc} since light is guided almost exclusively inside the dielectric gap, i.e., mostly outside the Si-area.

3. Waveguide Optimization

We base our hybrid silicon-plasmonic waveguide design on the generic planar conductor-gap-silicon (CGS) waveguide [7] and extend the dielectric and metal regions laterally. For the dielectric gap material, we select the DDMEBT nonlinear polymer [3] possessing linear and nonlinear indices of $n = 1.8$ and $n_2 = 1.7 \times 10^{-17}$ m^2/W, respectively, while the metal is silver for minimal Ohmic losses at $\lambda = 1550$ nm ($n_{\text{Ag}} = 0.14 - j11.4$). In order to boost the plasmonic confinement even further, we introduce an inverted metal rib [6] or wedge [8], laterally aligned with the underlying silicon waveguide [Fig. 1(a),(b)]. The corresponding intensity distributions (TM_{00} mode) are plotted

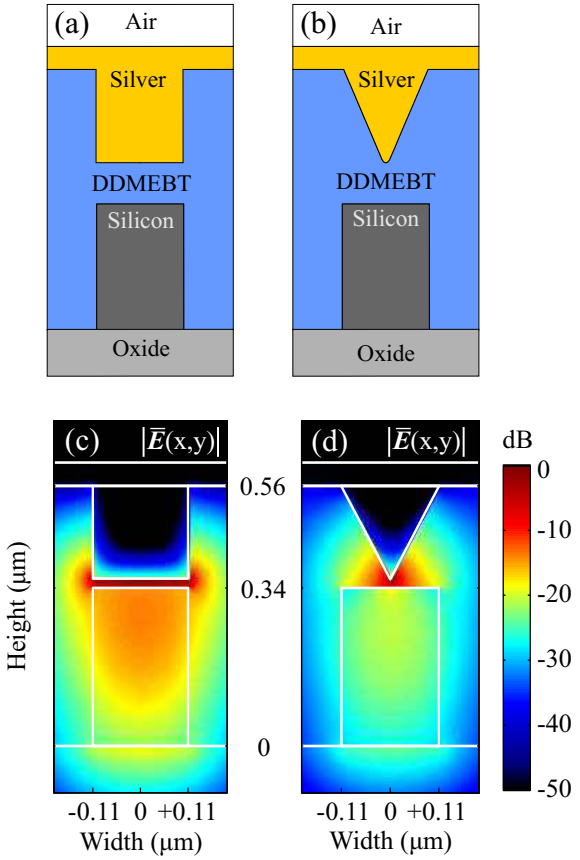

Figure 1: Cross-sections of (a) the inverted metal-rib and (b) the wedge hybrid silicon-plasmonic waveguide designs. (c) and (d): Typical intensity distributions at 1550 nm for the fundamental TM_{00} mode supported for a 20 nm gap. The nonlinear polymer is DDMEBT and the metal is silver.

in Fig. 1(c),(d). Other approaches are also possible for enhancing the mode confinement and improving the nonlinear response, for instance patterning the metal film into a stripe having a width comparable to the silicon wire or less.

The most crucial parameter of these hybrid silicon-plasmonic waveguide designs is the gap size (g). In Fig. 2 we plot both the nonlinear FoM ($\mathcal{F}$) and the FCE-scaling factor (f_{fc}) for a broad range of gap sizes (5–300 nm). One can readily confirm that the metal-wedge design offers considerable improvement in the FoM compared to the metal-rib designs as the gap decreases below 50 nm. The metal-rib designs exhibit an $\mathcal{F}$-peak at about 20 nm, and then the performance starts to drop as the losses become overwhelming. On the contrary, the $\mathcal{F}$ of the metal-wedge design continues to increase even below 5 nm gaps, owing to the enhanced field-confinement at the wedge-tip. As an example, for a gap of 20 nm the wedge design exhibits $\gamma \approx 6.7 \times 10^3$ m^{-1}W^{-1} (thus significantly outperforming standard SOI waveguides) and $L_{\text{prop}} \approx 43$ μm, amounting to $\mathcal{F} = 0.3$ W^{-1}. The factor f_{fc} is approximately 5×10^{-4}, which is orders of magnitude smaller than the f_{fc} exhibited by Si-wires, indicating that the relative importance of FCEs is rather limited. These figures can be further improved by

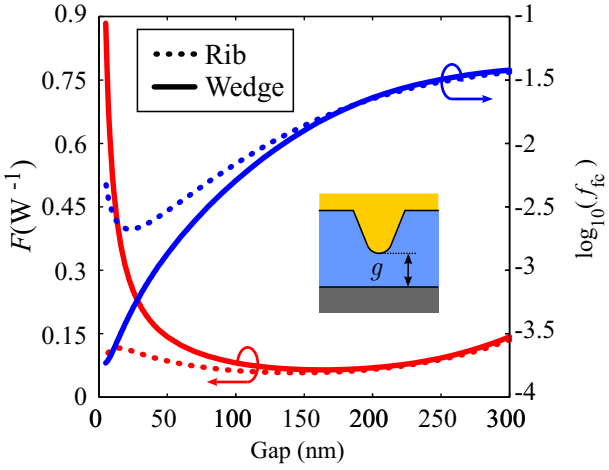

Figure 2: Nonlinear figure-of-merit $\mathcal{F}$ and FCE-scaling factor f_{fc} as a function of gap, for the two waveguide designs. The silicon ridge is in all cases $W \times H = 220$ nm $\times$ 340 nm, the silver film is 50 nm thick and the inverted metal-rib/wedge is $W \times H = 220$ nm $\times$ 200 nm. The wedge-angle is approximately 57° and its tip curvature is 1 nm.

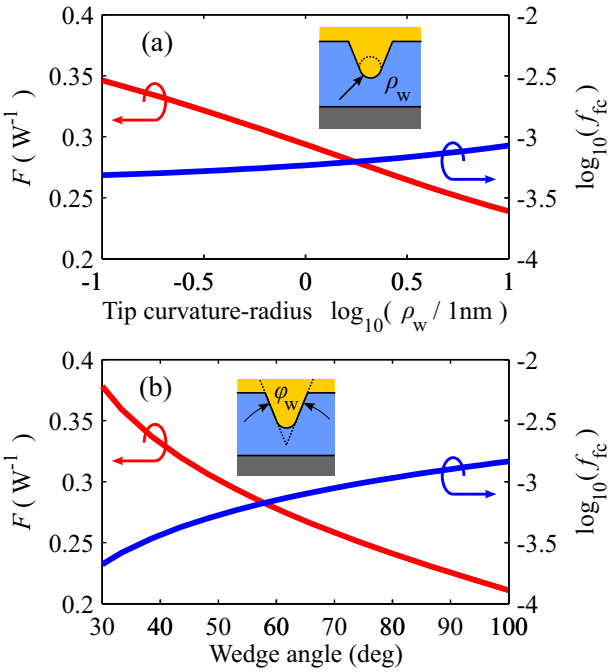

Figure 3: Nonlinear figure-of-merit $\mathcal{F}$ and FCE-scaling factor f_{fc} as a function of (a) wedge-tip radius for $\varphi_w = 53.2^\circ$ and (b) wedge-angle for $\rho_w = 1$ nm. The nonlinear gap is set at 20 nm, the silicon ridge is $W \times H = 220 \times 340$ nm^2, the silver film is 50 nm thick and the inverted metal-wedge height is 100 nm.

optimizing all waveguide parameters which can even lead to $\gamma > 10^4$ m^{-1}W^{-1}.

Focusing on the inverted metal-wedge design, it can be intuitively inferred that acute wedges will lead to improved performance, mostly thanks to the extreme field-confinement at the wedge-tip, which boosts the nonlinear-parameter since $\gamma \propto A_{\text{eff}}^{-1}$, where A_{eff} is the effective mode-area. To this end, we investigate the effect of the wedge-angle (φ_w) and its tip's curvature radius (ρ_w) on the resulting FoM. In our design, the nonlinear gap-size is set to 20 nm (being a reasonable compromise between mode confinement and fabrication challenge), the silicon ridge is set to $W \times H = 220 \times 340$ nm^2, the silver film is 50 nm thick and the inverted metal-wedge height (measured from the tip of the wedge to the bottom of the silver-film) is set to 100 nm. Varying φ_w is done by changing the wedge's lateral width, while varying ρ_w also amounts to a small change of the wedge-width in order to maintain the same wedge-height, wedge-angle and nonlinear-gap. The results are depicted in Fig. 3, where $\varphi_w = 53.2^\circ$ in Fig. 3(a) and $\rho_w = 1$ nm in Fig. 3(b). It is evident that the nonlinear figures-of-merit for HSP waveguides based on this design improve as the wedge becomes more acute, even though the increase is not as pronounced as with respect to the nonlinear gap. Additionally, it was found that obtuse wedges do no significantly restrict the performance; for instance, an acute wedge of $(\varphi_w, \rho_w) = (30^\circ, 0.1\text{ nm})$ leads to $\mathcal{F} > 0.6$ W^{-1} while an obtuse wedge of $(\varphi_w, \rho_w) = (100^\circ, 10\text{ nm})$ leads to $\mathcal{F} < 0.2$ W^{-1}. This means that the fabrication error-tolerance of this design is quite high and the penalty factor between the above two extreme combinations barely exceeds 3.

Finally, addressing some fabrication considerations, we note that the Si-rib width as well as possible lateral offsets between the wedge and the Si-rib do not have a major impact on the aforementioned figures-of-merit.

4. Validation

In order to validate the findings of the previous Section, we adopt the vectorial nonlinear Schrödinger equation (NLSE) framework of Daniel and Agrawal [2] that monitors the evolution of the field's complex-envelope along the waveguide. We calculate all parameters affecting the nonlinear response (losses, Kerr-effect, TPA and FCE) in terms of this NLSE formulation using our custom vector finite-element based mode-solver. Focusing on the CW or quasi-CW regimes, we drop all time-derivatives from the NLSE and record the nonlinear phase-shift ($\Delta\Phi_{\text{NL}}$) and the insertion-losses (IL) as a function of the input-power and the waveguide-length. The $\Delta\Phi_{\text{NL}}$ is extracted from the phase of the output-envelope and has positive contribution from the Kerr-effect ($\propto \gamma L_{\text{eff}} P_{\text{in}}$) and negative contribution from the FCD ($\propto f_{\text{fc}} L_{\text{eff}} P_{\text{in}}^2$); the latter tends to reduce the refractive-index inside silicon, proportionally to the TPA-generated free-carrier density, thus opposing the Kerr-effect which increases the refractive-index. The overall-IL are extracted from the amplitude of the output-envelope and depend on linear (ohmic, Rayleigh-scattering, surface-roughness) as well nonlinear loss-mechanisms, i.e. TPA and FCA.

Subsequently, we compare these CW-metrics for three nonlinear waveguides, namely our HSP-wedge design, a

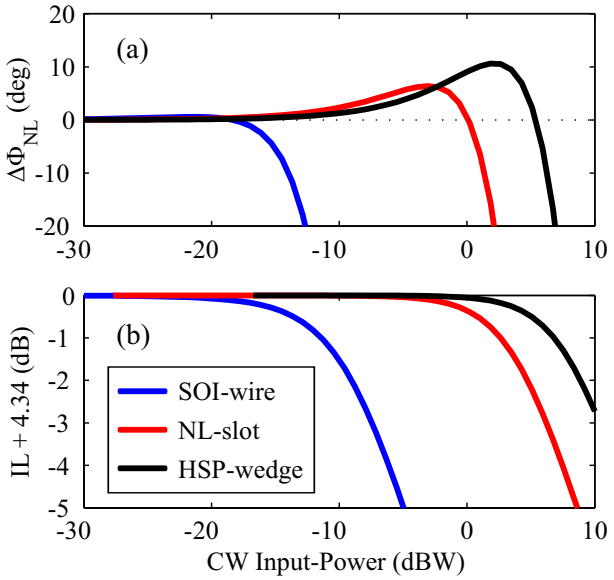

Figure 4: NLSE-calculated nonlinear (a) phase-shift and (b) insertion losses, as a function of the CW input-power along three waveguide designs of L_{prop} length. The SOI-wire is 400×340 nm^2 and operates in the fundamental TE-mode with nominal 1 dB/cm losses. The NL-slot is 140 nm-wide and formed between two 200×220 nm^2 Si-wires and operates in a TE-mode with nominal 1.6 dB/mm losses [3]. The HSP is made of a 20 nm gap separating a 200×220 nm^2 Si-wire from an Ag-wedge of 100 nm height with a tip-radius of 1 nm and operates in a TM-mode. The free-carrier effective lifetime was conservatively considered equal to 1 nsec in all three cases.

typical SOI-wire [2] and a nonlinear-slot [3]. For the purpose of comparison, the SOI-wire cladding and the nonlinear-slot are also filled with the same nonlinear polymer (DDMEBT) and the waveguide-length is equal to the L_{prop} of each design. In Fig. 4(a) we observe that the HSP has a higher FCD power-threshold than the SOI and slot design. This threshold can be defined as the power above which the negative-contribution of FCD overwhelms the positive one from the Kerr-effect, amounting to a negative slope in the $\Delta\Phi_{\text{NL}}$-vs.-P_{in} curve. For the HSP design this threshold-power is well above 0 dBW. The same holds true for the power-threshold associated with the nonlinear-IL, i.e., the overall-IL minus the linear-losses over $L = L_{\text{prop}}$, which amount to 4.34 dB. This power-threshold can be defined as the power where the nonlinear losses impose an additional 1 dB, i.e. $(\text{IL}+4.34) \approx -1$ dB, and is also well above 0 dBW for the HSP design. From Fig. 4 we can deduce that, in the CW-case, the power-threshold associated with FCD is generally lower, i.e. more strict, than the threshold associated with FCA. Let us finally note that the TPA-losses become important in much higher powers meaning that FCA is usually the dominant nonlinear loss mechanism. For the extrapolation of these remarks to the pulsed-regime, please refer to Section 5.

Finally, we note that these results for CW-radiation were corroborated by means of full-wave beam-propagation method simulations [9], and an excellent agreement between the full-wave method and the NLSE-approach was observed.

5. Discussion

The important attributes of the HSP nonlinear waveguide design, apart from being SOI compatible, are the very compact size, the high nonlinearity and the increased FCE power-threshold. The latter is crucial for Kerr-effect applications at interaction-lengths well below 1 mm. Assuming an effective free-carrier lifetime of 1 nsec [2], typical SOI waveguides have an FCE-ceiling in the order of 10 mW (CW), while the respective for HSP waveguides is above 1 W; this is reflected on the orders-of-magnitude smaller FCE-scaling factor f_{fc}. Moreover, SOI waveguides provide a higher FoM ($\mathcal{F} \approx 5$ W^{-1}), albeit on substantially longer length scales ($L_{\text{prop}} \approx 1$ cm). The interaction lengths can be reduced with nonlinear-slot designs [3] at the cost of a ten-fold decrease in $\mathcal{F}$. However, even though (or, exactly because) they avoid the metal-presence, these designs are still approximately two orders-of-magnitude longer than the respective HSP ones, and they achieve approximately equivalent figures-of-merit ($\mathcal{F}$ and f_{fc}). Finally, compatibility with the CMOS technology can be ensured, provided that the metal is changed from silver to copper. This is expected to marginally affect the nonlinear properties (γ), but cause a two-fold decrease of the propagation length (L_{prop}).

Evidently, the pulsed-regime performance will be considerably improved with respect to the FCE power-thresholds observed for the CW-regime. This is true for pulses with duration shorter than the carrier-lifetime ($\tau_{\text{fc}} \approx 1$ ns) and for low repetition-rates [10]. The reason behind this improvement is that even though the FCE are triggered instantaneously due to TPA, they are not given the time to considerably affect short-pulses due to their delayed response. In this manner, both FCD and FCA power-thresholds are at least 10–20 dB higher than the CW-ones, e.g. for guassian pulses shorter than τ_{fc}. This allows for higher powers and, consequently, much more pronounced Kerr-effect than the $\Delta\Phi_{\text{NL}} \ll \pi$ anticipated in the CW-regime [11]. Even for NRZ systems and/or high repetition-rates, the FCE power-thresholds are still higher than those calculated for CW-radiation. In overall, the estimates of Fig. 4, in and of themselves, are very pessimistic for most practical applications and mainly provide relative figures for the power levels at which FCE become important in different waveguide designs. Nevertheless, in the present work they can be employed as measures for comparative waveguide assessment and optimization, since it is well understood that the FCE-penalization always scales with the factor f_{fc}, in the pulsed as well as the CW-regime.

Ohmic heating of the structure is expected to arise when high optical power is launched into these nanoscale plasmonic waveguides [12], owing to the electric field penetrating its metallic areas. The generated heat is proportional to $\text{Im}\{n_{\text{Ag}}^2\}|\mathbf{E}|^2$, so, the increased confinement near the

metal/dielectric interfaces can potentially damage the device, especially for dielectric gap materials with low thermal conductivity and for acute metallic features. Additionally, the relatively slow temporal characteristics of thermal diffusion can impair transmissions in the pulsed regime. In this regard, it is essential that thermal exhaust channels, namely high thermal conductivity areas, are implemented in the waveguide cross section. These could include a thick and laterally extended metal cladding as well as a silicon slab, both compatible with the proposed HSP waveguide design. Finally, we anticipate that the thermo-electric properties of the materials involved will exhibit a significant dependence on their dimensions (thickness) and the fabrication process used [13], particularly for these nanophotonic waveguides. Attempts to rigorously quantify the impact of this phenomenon are currently under investigation.

6. Conclusion

We have investigated the potential of hybrid silicon-plasmonic waveguides for Kerr-effect applications in integrated photonic components. A set of figures-of-merit for the overall characterization of silicon-comprising nonlinear waveguides has been established, taking into account the two-photon absorption and free-carrier effects. Using these FoM, we have optimized an HSP waveguide design employing an inverted metal wedge and have acquired record-high nonlinear-parameter values approaching 10^4 $\mathrm{m}^{-1}\mathrm{W}^{-1}$. Furthermore, we have shown that the power-ceiling above which the FCE and TPA overwhelm the Kerr-effect is approximately two orders-of-magnitude higher compared to standard SOI waveguides. Finally, our findings have been corroborated with vectorial nonlinear Schrödinger equation techniques and full-wave beam-propagation numerical simulations, validating the proposed optimization approach.

Acknowledgement

This research has been co-financed by the European Union (European Social Fund – ESF) and Greek national funds through the Operational Program "Education and Lifelong Learning" of the National Strategic Reference Framework (NSRF) – Research Funding Program: Heracleitus II. Investing in knowledge society through the European Social Fund.

References

[1] Q. Lin, O.J. Painter, G.P. Agrawal, Nonlinear optical phenomena in silicon waveguides: Modeling and applications, *Opt. Express*, Vol. 15, No. 25, 16604–16644, 2007.

[2] B.A. Daniel, G.P. Agrawal, Vectorial Nonlinear Propagation in Silicon Nanowire Waveguides: Polarization Effects, *J. Opt. Soc. Am. B*, Vol. 27, No. 5, 956–965, 2010.

[3] C. Koos, P. Vorreau, T. Vallaitis, P. Dumon, W. Bogaerts, R. Baets, B. Esembeson, I. Biaggio, T. Michinobu, F. Diederich, W. Freude, J. Leuthold, All-Optical High-Speed Signal Processing with Silicon-Organic Hybrid Slot Waveguides, *Nat. Photonics*, Vol. 3, 216–219, 2009.

[4] M.L. Brongersma, R. Zia, J.A. Schuller, Plasmonics - The missing link between nanoelectronics and microphotonics, *Appl. Phys. A*, Vol. 89, No. 2, 221–223, 2007.

[5] R.F. Outlon, V.J. Sorger, D.A. Genov, D.F.P. Pile,X. Zhang, A hybrid plasmonic waveguide for subwavelength confinement and long-range propagation, *Nat. Photonics*, Vol. 2, No. 8. 496–500, 2008.

[6] A. Pitilakis, O. Tsilipakos, E.E. Kriezis, Nonlinear Effects in Hybrid Plasmonic Waveguides, in *Proceedings of 14th International Conference on Transparent Optical Networks*, Coventry, United Kingdom, July 2012, Art. No. 6254436.

[7] M. Wu, Z. Han, V. Vien, Conductor-Gap-Silicon Plasmonic Waveguides and Passive Components at Subwavelength Scale, *Opt. Express*, Vol. 18, 11728–11736, 2010.

[8] A. Boltasseva, V.S. Volkov, R.B. Nielsen, E. Moreno, S.G. Rodrigo, S.I. Bozhevolnyi, Triangular metal wedges for subwavelength plasmon-polariton guiding at telecom wavelengths, *Opt. Express*, Vol. 16, No. 8, 5252–5260, 2008.

[9] O. Tsilipakos, A. Pitilakis, A.C. Tasolamprou, T.V. Yioultsis, E.E. Kriezis, Computational Techniques for the Analysis and Design of Dielectric-Loaded Plasmonic Circuitry, *Opt. Quant. Electron.*, Vol. 42, 541–555, 2011.

[10] L. Yin, G.P. Agrawal, Impact of two-photon absorption on self-phase modulation in silicon waveguides, *Opt. Lett.*, Vol. 32,No.14,2031–2033, 2007.

[11] E. Dulkeith, Y.A. Vlasov, X. Chen, N.C. Panoiu, R.M. Osgood, Jr., Self-phase-modulation in submicron silicon-on-insulator photonic wires, *Opt. Express*, Vol. 14, No. 12, 5524–5534, 2006.

[12] D. Perron, M. Wu. C. Horvath, D. Bachman, V. Van, All-plasmonic switching based on thermal nonlinearity in a polymer plasmonic microring resonator, *Opt. Lett.*, Vol. 36, No. 14, 2731–2733, 2011.

[13] G. Chen, P. Hui, Thermal conductivities of evaporated gold films on silicon and glass, *Appl. Phys. Lett.*, Vol. 74, No. 20, 2942–2944, 1999.